Crossover from Unentangled to Entangled Dynamics in a Systematically Coarse-Grained Polystyrene Melt

Qi Sun and Roland Faller*

Department of Chemical & Materials Science, University of California Davis, Davis, California 95616

Received July 7, 2005; Revised Manuscript Received November 18, 2005

ABSTRACT: We develop a mesoscale polystyrene model based on atomistic simulations of oligomers using the iterative Boltzmann inversion method. The potential is optimized against the atomistic simulation until the radial distribution function generated from the mesoscale model is consistent with the atomistic simulation. The mesoscale model allows to elucidate the polymer dynamics of long chains. The dynamics of polystyrene melts are investigated at various chain lengths between 15 and 240 monomers. Mean-squared displacements are analyzed to capture the dynamics changing from the Rouse to the reptation behavior. The reorientation behavior of segmental vectors is investigated to identify the heterogeneity along the chain. Diffusion constants of various systems are calculated to verify the crossover from the unentangled to entangled dynamics. Rouse mode analysis shows that the Rouse model is applicable from chain length between 50 and 100 monomers. The entanglement length of this polystyrene model is around 85 monomers at 450 K, in fair agreement with experiments.

1. Introduction

To investigate the behavior of polymer systems on the local scale, atomistic simulations are required. To understand the many rules governing material properties of polymer systems, it would be highly desirable to have a multiscale model which can include all relevant interactions.[1] Experimental techniques such as NMR spectroscopy,[2−4] atomic force microscopy,[5] position annihilation spectroscopy,[6] and dielectric spectroscopy[7] have been developed to obtain a detailed description of the static and dynamic properties of polymeric systems from local chain arrangements up to the behavior of the polymeric materials in macroscale applications. Techniques covering the whole range of length scales together do not exist in computer simulation to date. Some phenomena, for example entanglements, occur on length scales not accessible by fully atomistic simulations.

In view of these considerations, there are many efforts to devise simulation techniques, which coarsen the microscopic models in a more or less systematic way. There is a significant tradition of simulations of simplified polymer models originating from statistical mechanics, which provide a powerful basis for the investigation of local and dynamical properties ranging from single chain systems to polymer solutions, melts, and other systems.[8−12]

Coarse-graining, the systematic mapping of various length scale models onto each other, has made significant progress in modeling polymer systems.[13−22] A newly developed technique, the "iterative Boltzmann inversion" (IBI), also known as the "inverted Boltzmann method",[23] can be used to generate meaningful potential parameters during coarse-graining. It employs the differences in the potentials of mean force between the distribution functions generated from a trial potential and the true (simulated) distribution functions to improve the effective potential until the radial distribution function (RDF) generated from the mesoscale simulation is consistent with the atomistic simulation. IBI has been successful in the mapping of pure polymer systems;[13,23] however, it has not yet been used to describe an entangled polymer system. We aim at filling this gap. By connecting different models, we can gain insight into interactions of various length scales at once with reasonable computer power.

Several researchers have dealt with detailed simulations of polystyrene (PS) melts[24−29] and the entanglement behavior of polymers.[8,9,30,31] But, there is not yet a computational analysis of the entanglement length of PS, since the equilibration process is too long for polymer systems with hundreds of monomers. Dynamical problems in polymer melts arise from the very nature of the polymer: polymers are one-dimensional connected objects and cannot cross each other. The Rouse and the reptation model are two of the most prominent dynamical models in describing the motion of the polymers. The Rouse model[32] treats the polymer as a set of noninteracting beads connected by springs. The dynamics of polymer chains in a melt is governed by a viscous force and the tensile forces arising in stretched parts of the chain. The reptation model confines the movement of the polymer to a tube and describes global dynamic problems (cf. Figure 1). Mean-squared displacements of the monomers $\mathbf{g}'_1(t)$ are important in characterizing polymer dynamics: (a) For very short time $t < \tau_e$, the segment does not feel the constraints of the tube, so the actual dynamics correspond to the Rouse model. (b) For $\tau_e < t \leq \tau_R$, the motion perpendicular to the primitive path is restricted, but the motion along the primitive path is free. (c) For $\tau_e < t \leq \tau_d$, the internal degrees of freedom are relaxed but the chains still are confined to the tube. (d) For $t > \tau_d$, the dynamics is governed by reptation. All these processes can be summarized as follows:[33,34]

$$\mathbf{g}'_1[t] = \begin{cases} Nb^2(t/\tau_R)^{1/2} & t < \tau_e \\ Nb^2(t/Z^2\tau_R)^{1/4} & \tau_e < t \leq \tau_R \\ Nb^2(t/\tau_d)^{1/2} & \tau_R < t \leq \tau_d \\ Nb^2(t/\tau_d) & t > \tau_d \end{cases} \quad (1)$$

τ_e, τ_R, and τ_d are the entanglement time, Rouse time, and disengagement time, respectively. N is the number of links along a chain, b is the effective link length, and Z is the number of steps in a primitive chain. In the Rouse model only mean-squared displacement behaviors with exponents of 1/2 and 1 are contained as the only subdiffusive process is the motion of a monomer against the center of mass of the chain at short times. These two models serve as the theoretical basis of our

10.1021/ma0514774 CCC: $33.50 © 2006 American Chemical Society
Published on Web 12/20/2005

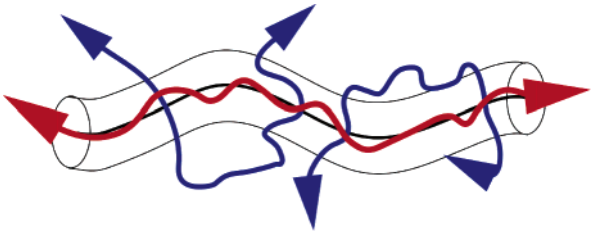

Figure 1. Illustration of two dynamic movements from Rouse model and the reptation model. The red color represents the two-dimensional movement from the confinement of a "tube" captured by the reptation model, and the blue color represents the free three-dimensional movement assumed by the Rouse model.

simulations. The entanglement length can be employed to mark the transition from the Rouse to the reptation model with increasing chain length. Though the reptation model is successful, our present understanding of the dynamics in entangled systems is still incomplete. The aim of this project is to determine the onset of entanglements in a systematically coarse-grained polystyrene model.

Starting from the atomistic model of pure polystyrene with 48 chains, we investigate the local structure, particularly the radial distribution function (RDF) and the bond and angle distributions. These parameters, together with the effective nonbonded potentials derived by the IBI, comprise the force field of the mesoscale model. We observe the dynamic behaviors of the mesoscale model and obtain the entanglement length of PS.

2. Simulation Investigations

2.1. Atomistic Simulation. Atactic PS systems with 48 chains of 15 monomers are investigated in atomistic details to obtain the input parameters for the mesoscale model. Our simulations contain 48 chains with completely random tacticities. The probability of a meso or racemo dyad at any given position is equal. The simulation is conducted at 450 K for 20 ns. For the force field of PS, we use the Lennard-Jones parameters of Jorgensen and Severance.[35] The bending potential from all the angles, the torsion potentials for all the backbone and phenyl ring carbons, and the improper potential are taken from refs 36 and 37. All bonds are constrained, and all 1−4 nonbonded interaction are excluded. Atomistic simulations are performed using MD at a pressure of 101.3 kPa. Constant temperature and pressure are ensured using Berendsen's method[38] with time constants 0.2 ps for temperature and 1.0 ps for pressure, respectively. A compressibility of 1.12×10^{-6} kPa^{-1} is applied to the three Cartesian directions independently. Simulations are performed using the Gromacs molecular simulation package[39] with a time step of 0.002 ps, and configurations are saved every 2000 steps.

2.2. Mapping. The mapping is an interplay between atomistic and mesoscale models. The input parameters of the mesoscale model are optimized against the "correct" results from the atomistic scale. To map atomistic to mesoscale models, one groups several atoms together into "superatoms". Superatom centers are chosen in order to produce a single peaked bond distribution on the mesoscale leading to a harmonic bond.[40] Further details of the mapping can be found in ref 41. Here we summarize only the main findings. We group the 16 atoms of a monomer together and the superatom centers of PS have been placed on the carbons connecting the backbone with the side ring.

The angle distribution and the corresponding forces of the mesoscale model are derived from the atomistic model as well. The angle histograms can be calculated by obtaining trajectories only containing the superatoms. A torsion potential is not needed.

The nonbonded interaction parameters are crucial in obtaining a successful mesoscale model. The IBI[23] is used to reproduce the structure by means of radial distribution functions. The numerical potentials are optimized iteratively until the desired distributions of the coarse-grained model and the atomistic model coincide within a reasonable tolerance. It is worth stressing two points: First, on the scale of the nearest neighbors the local packing of interaction centers is the strongest effect, so the optimization of the potential should focus on the local interactions. Second, during the iteration process, it is efficient to apply a multiplicative factor to the correction term as the iteration nears the end. The factor is any number between 0 and 1, whose magnitude depends on how far the resulting RDF deviates from the atomistic RDF. We used factors between 0.05 and 1. In some cases simulations with different factors have been performed for the same iteration in parallel, and the most successful, i.e., the one yielding the RDF closest to the target, has been chosen as the starting point for the next iteration.

2.3. Mesoscale Simulation. The molecular dynamics program MDspherical is applied in the *NVT* ensemble for the mesoscale simulations.[42] The reduced temperature ($T^* = k_B T/\epsilon$) is set to 1. σ^* is set to 1 nm. The density is 5.7499 monomers/σ^3, corresponding to 978 kg/m^3. The temperature is maintained by a Langevin thermostat with a friction constant $\Gamma = 1.0\tau^{-1}$, where $\tau = \sqrt{\sigma^2 m/\epsilon}$.[43] The systems consist of an orthorhombic box employing periodic boundary conditions. The equation of motion is integrated with a time step $\Delta t = 0.01\tau$, and trajectories are stored every 2000 steps. The bond length is 0.2545 nm with a strength of 0.03 kJ/mol. The cutoff for the nonbonded interactions is 1.805σ. The box size is changed according to the fixed density. The numerical potential of mean force, which comes from optimization to systems of the pure 48 chains 15-mer, is applied to all systems. The details of the investigated systems are listed in Table 1. We are aware that the largest systems have to be analyzed with caution due to the system sizes.

The initial configuration of the system of 48 15-mer chain comes from the atomistic scale simulation. Using bond, angle, and torsion parameters from the atomistic scale, a mesoscale model consisting of 48 chains 15-mer is set up. Energy minimization is applied to get rid of initial overlaps. All longer chain systems are set up based on the 48 chains 15-mer. Take an example of 48 chains 30-mer: Starting from the 48 15-mer system, the initial configuration of 30 mers is generated by a translation of a copy of the 15-mer system, and then the translated and the original 15-mer configuration are put together in a new box which is expanded at a fix density and generates a new initial configuration of 96 chains of 15-mer. By connecting nearby chain ends, the 96 chains of length 15 can successfully generate 48 chains of 30 monomers each. Equilibration can be checked if the end-to-end vectors are completely relaxed. Static properties, for example, radius of gyration, are used to validate the mesoscale model.

Entanglements constitute a major feature of the dynamics of long polymers. Our project focuses on describing entanglement behavior by several manifestations, in particular mean-squared displacements, reorientation of local vectors along the backbone, the Rouse plateau in the chain length dependence of the diffusion constant, and Rouse mode analysis.

Table 1. Simulation Details and Characterization Properties of the Different Systems[a]

			characterizations			
N_C	N_P	t_{sim}	$\langle R_g^2 \rangle$	$\tilde{l}$	R_k	τ_{end}
15	48	200	0.52 ± 0.08	0.55 ± 0.08	0.57 ± 0.09	9 ± 1
30	48	1000	1.39 ± 0.13	0.68 ± 0.10	0.69 ± 0.06	48 ± 10
40	48	10 000	2.10 ± 0.18	0.69 ± 0.11	0.85 ± 0.07	120 ± 20
50	48	10 000	2.79 ± 0.18	0.70 ± 0.10	0.90 ± 0.06	152 ± 23
70	48	20 000	4.26 ± 0.53	0.71 ± 0.12	0.93 ± 0.10	395 ± 40
80	48	20 000	5.01 ± 0.59	0.71 ± 0.15	0.93 ± 0.09	438 ± 45
90	48	20 000	5.72 ± 0.60	0.72 ± 0.10	0.98 ± 0.11	644 ± 60
100	48	30 000	6.09 ± 0.94	0.71 ± 0.09	0.95 ± 0.14	689 ± 70
120	24	40 000	8.21 ± 1.47	0.72 ± 0.11	1.04 ± 0.08	1196 ± 100
160	24	40 000	11.20 ± 1.70	0.76 ± 0.09	1.05 ± 0.15	5010 ± 540
240	12	80 000	17.53 ± 3.48	0.72 ± 0.10	0.92 ± 0.18	25 900 ± 2500

[a] N_C is the chain length; N_P is the number of polymer chains; t_{sim} is the simulated time for the systems. The units of $\langle R_g^2 \rangle$, $\tilde{l}$ or R_k, and τ_{end} are nm^2, nm, and time units.

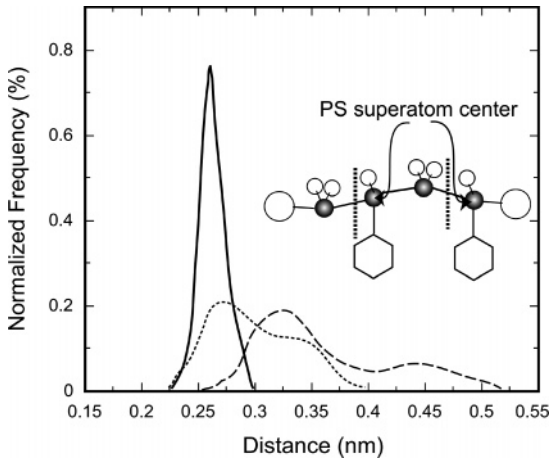

Figure 2. Histogram distribution from different center of mass.

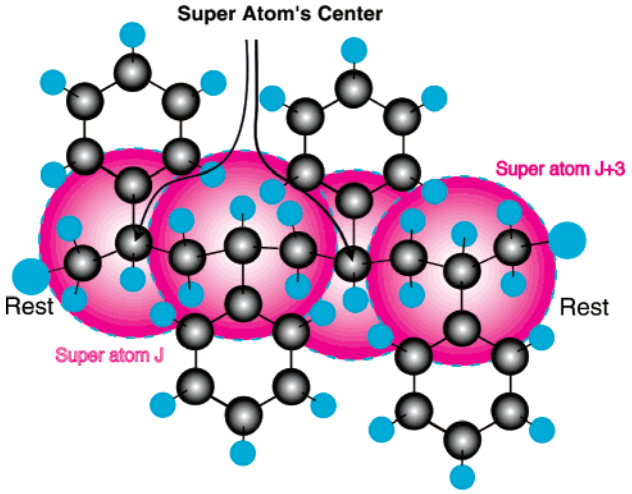

Figure 3. Atomistic structure of PS and its mapping to a mesoscale model.

3. Results and Discussion

3.1. Mapping. The histograms of superatom centers from the backbone carbon connected to the pendant group, the phenyl carbons connected to the backbones, and the center between the two are plotted in Figure 2. Only the centers of the backbone carbons connecting the phenyl groups result in a single harmonic peak, so one superatom represents 16 atoms with a center at the backbone carbon connected to the side rings as shown in Figure 3. The angles range from 77° to 180°, and the angle distribution has two peaks at 110° and 150° (cf. Figure 4a).

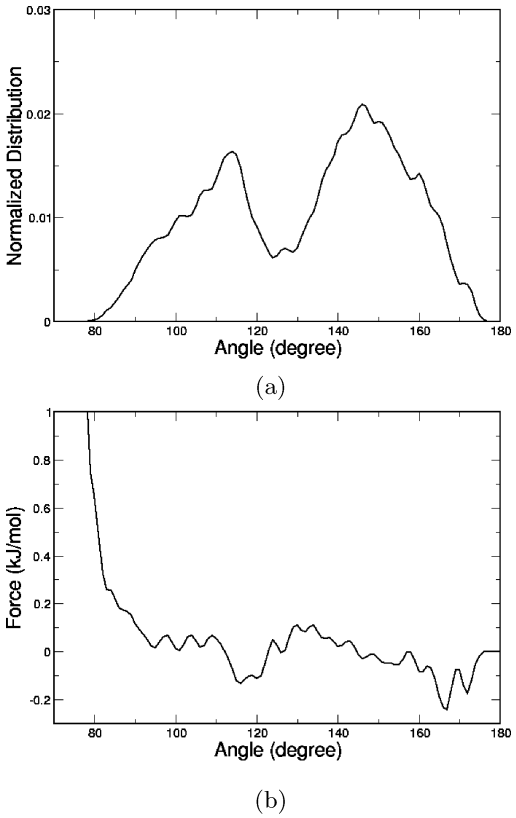

Figure 4. Angle distribution (a) and angle force (b) of mesoscale PS model at different angles.

The corresponding force is plotted in Figure 4 as well. Angles lower than 77° are assigned forces which gradually increase to the maximum of 50 kJ/mol rad^2.

Figure 5 depicts sample RDFs along the iteration of the nonbonded potential. After about 25 iterations, the RDF is consistent with the atomistic one within tolerance. IBI proves to be an attractive solution for deriving effective potentials during mapping atomistic scale to mesoscale.

3.2. Statics and Dynamics of Mesoscale PS. Extensive simulations of systems with chain lengths ranging from 15 to 240 monomers provide an approach to capture the emergence of the reptation behavior and the entanglement length of PS. First, static properties of PS are investigated to verify our mesoscale model including radius of gyration R_g, persistence length $\tilde{l}$, and Kuhn length R_k. The dynamics is investigated by the correlation time of end-to-end vectors (τ_{end}), mean-squared displacement, reorientation behaviors, diffusion constants, and Rouse mode analysis.

CDV

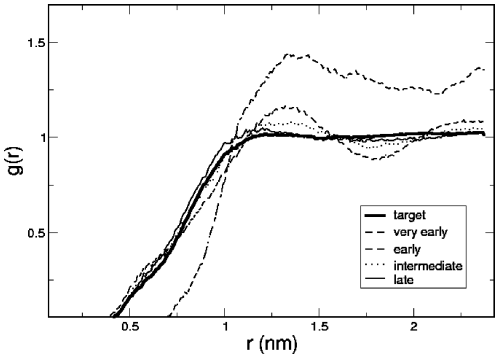

Figure 5. Illustration of the various stages in the iteration process by the iterative Boltzmann inversion.

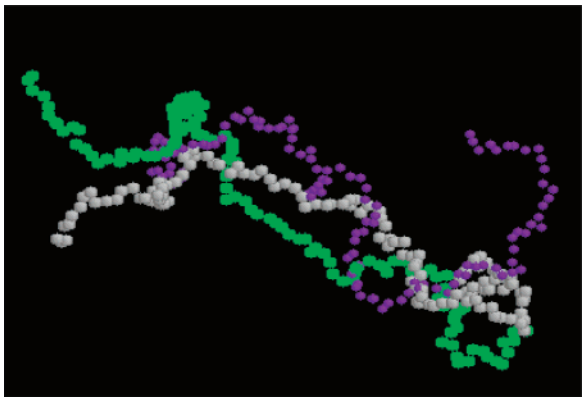

Figure 6. 3-D visualization of the reptation tube for the system of chain length 120-mer. The snapshots are recorded at time interval of 1000 time units.

3.2.1. Statics. Snapshots of one 120 monomer chain at different times are provided in Figure 6. It is clearly observed that some part of the chain takes on free diffusion while most of it is still confined in a tube like region. The program Rasmol is used for the visualization.[44]

The size of the polymer can be appropriately represented by the gyration radius R_g defined as

$$R_g = \sqrt{\frac{1}{N}\sum_{n=1}^{N}\langle (R_n - R_{cm})^2\rangle} \qquad (2)$$

where R_{cm} is the position of the center of mass of the chain and R_n is the position of the nth monomer. The gyration radii at different chain lengths are calculated and listed in Table 1. It shows clearly that the square of the radius of gyration increases linearly with the number of monomers N indicative of a random walk.

Real polymers have more or less flexibility. Let $R(s)$ be the position of a point on the polymer contour at position s. The vector $u(s) = \partial R/\partial s$ is a unit vector tangent to the chain. The persistence length measures the length along the chain over which the tangent vectors decorrelate. The orientational correlation functions of $u(s)$ decay exponentially along the chain in the wormlike chain picture[45] as

$$\langle u(s)\cdot u(0)\rangle = \exp(-s/\tilde{l}) \qquad (3)$$

The characteristic length of this decay, $\tilde{l}$, is called persistence length of the chain. At $s \ll \tilde{l}$, the chains can be considered as rigid rods, and at $s \gg \tilde{l}$, the chain describes a random walk. To understand the flexibility of PS chains, the persistence length at various chain length are measured and also listed in Table 1.

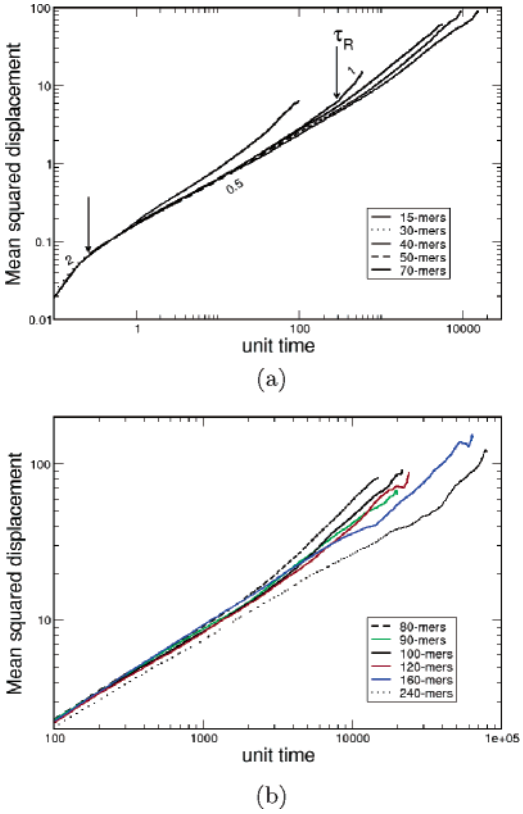

Figure 7. Time dependence of mean-squared displacements of monomers in the central part of the chains: (a) chain length of 15, 30, 40, 50, and 70; (b) chain length of 80, 90, 100, 120, 160, and 240.

The Kuhn length R_k, which is defined by

$$R_k = \frac{\langle R^2\rangle}{N l_b^2} \qquad (4)$$

where l_b is the distance between neighbors, also characterizes the stiffness of a given polymer chain; stiffer chains have larger R_k. Both persistence length and Kuhn length are independent of chain length for systems of chain length over 50.

3.2.2. End-to-End Reorientation. The end-to-end vectors as the primary vectors of the polymers have the longest relaxation time. The correlation times of end-to-end vector (τ_{end}), which indicate that our polymer chains are fully relaxed, are calculated and listed in Table 1 as well. Here we see that for long chains the reorientation times increase clearly stronger than with N^2 already indicating onset of entangled behavior. Note that τ_{end} is calculated from the second-order Legendre polynomial and therefore can be shorter (by a factor of 2−4) than some of the Rouse times below.

3.2.3. Mean-Squared Displacement. We use the mean-squared displacement of monomers $\mathbf{g}'_1[t]$ to investigate the motion of superatoms. To minimize end effects, we focus on the central monomers. Figure 7 shows the resulting MSDs for chain length from 15 to 240 monomers. Table 2 summarizes the characteristic times determined by the first-order derivative along the MSDs. Figure 8 gives examples of obtaining the entanglement time, Rouse time, and disengagement time using the derivative of the log of the MSD. The 90-mer takes on a free movement inside a tube and then feels the constraints from the tube and eventually free diffusion. As these chains are short, we do not reach the theoretical values of the exponents but we can distinguish different regimes. The movement of 50-mers is first constrained by connecting monomers and further diffuses

CDV

Table 2. Rouse Times τ_R of Various Systems of Rouse Model Behaviors and Entanglement Time τ_e, Rouse Time τ_R, and Disengagement Time τ_d of Various Systems Exhibiting Reptation Behavior[a]

	Rouse model			reptation model			
N_C	τ_R	τ_R/N^2	N_C	τ_e	τ_R	τ_R/N^2	τ_d
15	37 ± 15	0.333	90	854 ± 68	1456 ± 180	0.180	2289 ± 340
30	254 ± 29	0.282	100	930 ± 75	1890 ± 320	0.189	3879 ± 230
40	315 ± 50	0.197	120	975 ± 40	2150 ± 330	0.149	5325 ± 365
50	620 ± 90	0.248					
70	986 ± 124	0.201					
80	1168 ± 102	0.183					

[a] We clearly see entanglements also for the longer chains, but the determination of times is ambiguous.

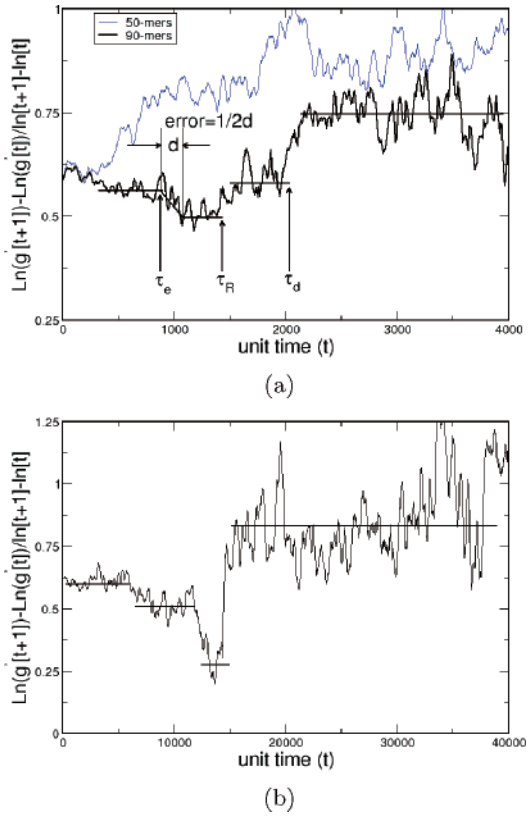

Figure 8. First-order derivative of logarithmic MSDs dependent on unit time at various chain lengths: (a) chain lengths of 50 and 90; (b) chain length of 160 monomers.

together globally while the 160-mer chains have still not yet arrived at free diffusion at unit time of 4000 but at about 10 000 time units a clear slowdown for a short dynamic regime is observed. It is worth mentioning that while this approach is crude, it is superior to assigning such times by direct visual observation. The error is taken as the half time difference between two successive fluctuation regions. Table 2 shows that the Rouse and disengagement times are strongly dependent on chain length while the dependence of the entanglement times is weaker. For the chains of 15 monomer it is difficult to identify a clear Rouse regime as the minimal exponent is 0.75, which is confined between the ballistic motion corresponding to an exponent of 2 and free diffusion. The initial dynamic regime for chains of length 30−70 shows a logarithmic slope of 0.6, and the kink marks transition from a power of 0.6 to 1. The slope changes at longer times as the chain length increases. It is predicted by the Rouse model that $\mathbf{g'}_1[t] \propto t^{1/2}$ to $\mathbf{g'}_1[t] \propto t^1$ at the Rouse time which should be proportional to N^2. As the Rouse time is normalized by N^2, fluctuations around a constant number of 0.2 are observed from chain length 40−160 monomers. For chain length 90 and longer increasing influence of reptation can be observed. Initially all curves obey the same dynamics $\mathbf{g'}_1[t] \propto t^{1/2}$ up to about 1000 time units and then kink down to smaller slopes.

Gradually the curves kink up to a power of 1/2 and further to a slope 1, indicating free diffusion. As seen in Figure 7, the slowdown below the Rouse dynamics is clearly identified, and the longer chains exhibit a clearly lower slope than those of shorter chains. This is not surprising as it is well-known that the crossover behavior in the transition to reptation often obscures the transition almost completely.[9] Take the chain length of 160 as an example; an initial slowdown identified with the entanglement onset which, however, does not completely drop from $\mathbf{g} \propto t^{1/2}$ to $\mathbf{g} \propto t^{1/4}$ is at around time 1100, which means the motion of the monomers is constrained orthogonally to the primitive path of the tube. At longer times (<15 000) a slope of 0.25 is identified. The chains with 90 or 100 monomers at this time already move out the tube and take on free diffusion. At about 15 000 time units the chains of 160 monomers escape the constraints of the tube, while the relaxation of 240 monomers is still in the tube.

The transition from the Rouse model to the reptation model determines the entanglement length. Our initial investigation of the mean-squared displacement indicates that the entanglement length of PS is about 80−90 monomers. Experiments determine N_e by measuring the plateau modulus under oscillatory shear. This yields a $N_e \approx 130$ for PS.[46] This number is at 413 K, but the difference to 450 K is expected to be minor. It is known that geometrically defined entanglement lengths are often shorter than rheological experiments.[8] Our simulation data can also be compared to a simple simulation model of polymers with stiffness.[10] This model was not optimized against any specific polymer but is characterized by a persistence length. The entanglement length $N_e = 8$ for the chain with a similar persistence length $\tilde{l} = 3$ is much smaller compared to our result of $N_e = 80$. We see that our mesoscale model provides a much better estimate of N_e than the simple model in comparison to experiments. This improvement can be explained by that an extensive numerical potential is employed other than a purely repulsive Lennard-Jones potential used in the simpler model.

3.2.4. Reorientation Behaviors. The reorientation correlation function can be defined by the second-order Legendre polynomial as

$$P_2(t) = C_{reor} = \left\langle \frac{1}{2}[3(\vec{u}(t)\vec{u}(0))^2 - 1] \right\rangle \qquad (5)$$

It is used as a measure of chain dynamics, where $\vec{u}(t)$ and $\vec{u}(0)$ are unit vectors. The second-order polynomial is chosen because it has head-to-tail symmetry along the chain and its integral can be measured directly from NMR experiments.[2] It is known that chain stiffness and chain length contribute to reorientation properties of polymers.[11] Since the same potential is applied

CDV

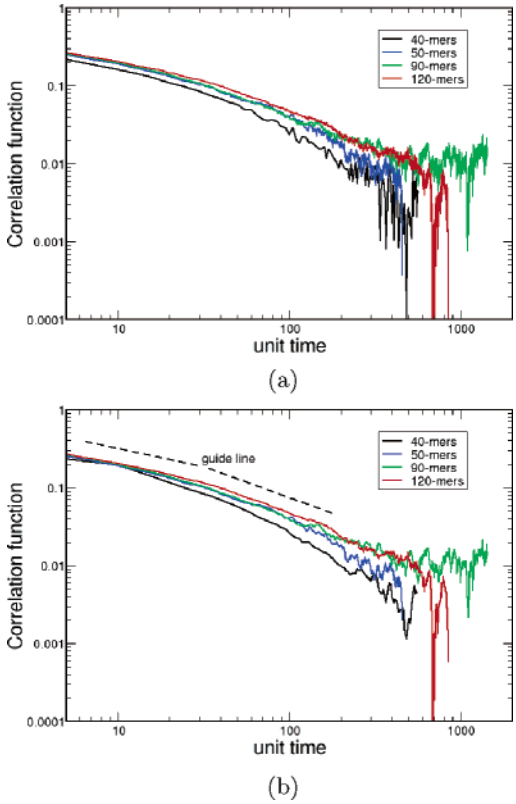

Figure 9. Time dependence of second-order Legendre polynomial of local vectors at chain length of 40, 50, 90, and 120 monomers: (a) raw data; (b) running time average of 5 with guide lines.

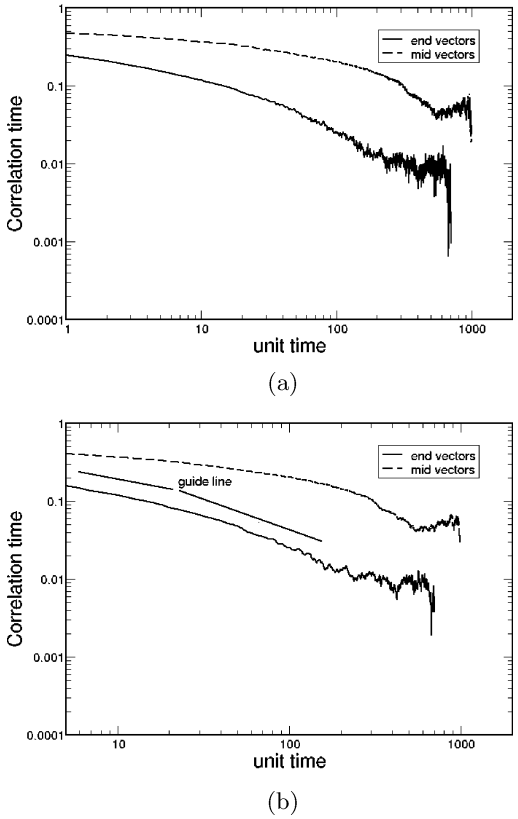

Figure 10. Depiction of end effects at chain length of 40 monomers: (a) raw data; (b) running time average of 5 with guide lines.

and we verified the persistence lengths is almost constant with chain length in all simulations, we focus on the reorientation dependence with chain length. We use local vectors to explore the orientation behaviors. Selected correlation functions are shown in Figure 9 for vectors connecting superatoms three bonds apart. To minimize the noise of the statistics, running averages of length 5 are plotted as well as the raw data. Reorientation correlation functions decay slower with increasing chain length. Overall, a two-stage reorientation is clearly visible. The first stage which looks like an algebraic decay occurs on times scales of 10−100 time units. On this time scale, the vectors do not feel the polymeric identity as it is clearly shorter than any times calculated above. Correlation functions of shorter chains bend over to a second algebraic process quite soon. For short chains, the local process is also more effective since it correlation function decays to lower values as longer chains have more residual orientation when the second process sets in.

The reorientation of chains of length 40 is taken as an example to show the heterogeneity of segmental motion along the chain. The first-order Legendre polynomial is plotted against time in Figure 10. The three vectors closest to either chain end and the middle three vectors are used to characterize the difference in local dynamics. End vectors reorient much faster at both short and long times. Movements from middle monomers are constrained by connecting monomers from both sides which need more time to relax. The ends of polymers are always the starting points of the reorientation and bear less confinement compared to the middle monomers. This has been observed in atomistic simulations as well.[47] Even when the motion is constrained by reptation the ends are free.

3.2.5. Diffusion Constants. Entanglement lengths can also be determined from diffusion constants.[10,34] For $t \geq \tau_R$, the diffusion constants of the polymer is defined by

$$D_{\text{diff}} \approx \lim_{t\to\infty} \frac{\langle (R(t) - R(0))^2 \rangle}{6t} \tag{6}$$

where $R(t)$ is the position of center of mass at time t. The diffusion constants can be calculated as one-sixth of the slope from the linear fit to MSDs starting after the longest relaxation time. Table 3 shows the diffusion constants for various chain length. We observe that the diffusion slows down with increasing chain length consistent with entanglements. In the Rouse picture the diffusion constant would decrease with the size of the chain, i.e., the square of the gyration radius and thus linear with chain length for chains performing a random walk.

Table 3. Diffusion Constants (6DN) of PS Chains at Various Chain Lengths

N_c	D (10^{-5} cm^2/s)	6DN	N_c	D (10^{-5} cm^2/s)	6DN
15	9.983	898.5	80	0.896	430.1
30	2.904	522.7	90	0.691	373.1
40	1.955	469.2	100	0.607	364.2
50	1.457	437.1	120	0.403	289.8
70	1.015	426.4	160	0.256	245.9

In Figure 11 we find a plateau between 40 and 80 monomers representing this behavior. With the onset of entanglements, the diffusion coefficient drops to $D \propto N^{-2}$. The crossover from the plateau to the linear decay in $6DN \sim N$ represents the entanglement length which again is between 80 and 90 monomers, consistent with our earlier analysis. The data for the two shortest chain systems, especially the 15 monomer chains, deviate from this plateau behavior; this discrepancy can be explained by the chain length of these two system. They are still oligomers. We cannot assume that these chains perform a random walk which is necessary for the linear decay in the diffusion constant. This is consistent with our analysis in Table

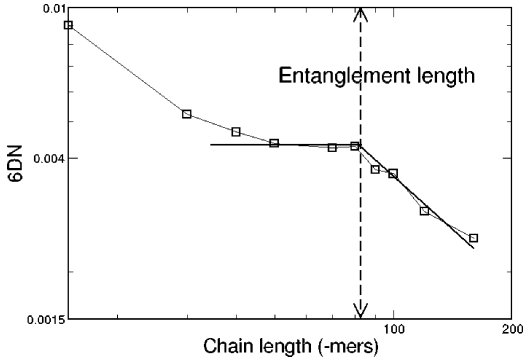

Figure 11. Diffusion constants at various chain length.

1 where we found shorter Kuhn lengths and persistence lengths for these chain lengths. We see that the Rouse model is applicable only in a specific chain length range which was found earlier in a study of chains of different stiffness.[10,11] The same behavior has been observed for systematically coarse-grained PI.[13] With increasing stiffness the whole existence of the Rouse plateau becomes questionable.

3.2.6. Rouse Mode Analysis. According to the Rouse model, the normalized autocorrelation function of all Rouse modes collapse onto a master curve for one system if time is rescaled by the square of the mode number. The Rouse modes or normal coordinates X_p are defined by

$$X_p = \frac{1}{N}\int_0^N \mathrm{d}n \cos\left(\frac{p\pi n}{N}\right) R_n(t) \tag{7}$$

with the autocorrelation functions obeying

$$\langle X_p(t)\, X_p(0)\rangle / \langle X_p{}^2(0)\rangle = \exp(-t/(\tau_1/p^2)) \tag{8}$$

in the Rouse regime.

The normal coordinate X_p represents the internal conformation of the polymer. This analysis is a clear test to which extent the Rouse model is applicable for a given system. p is the mode index. The mode with index 0 relates to the diffusive center of mass motion and is not expected to decay exponentially, $p = 1$ is the internal mode corresponding to the end-to-end motion, $p = 2$ represents motion on the scale of half the chain, $p = 3$ on the third of the chain, and so on. The higher p, the shorter the length scale. To decide whether the Rouse model is the appropriate description of a polymer system, it is necessary to calculate the modes. To test for Rouse behavior, chain lengths of 40−240 monomers are analyzed. The short ones have been ruled out already due to their diffusion behavior. Figure 12 is the Rouse model analysis of 40, 70, and 80 monomers and Figure 13 of 100, 120, and 240 monomers. We clearly observe that the Rouse modes change from a scattered pattern to a master curve at 80 monomers and differentiate again in the case of 100. Following the above equation, it is expected that the different modes should collapse onto a single curve if time t is scaled by p^2 from the Rouse model. For chain length of 40 monomers, it is still too short to apply the Rouse model. As the chain length at 70 or 80, the data collapse nicely onto a single curve, which is consistent with for all the chain length lower than entanglement length, the Rouse model being valid. As the chain length increases further to 100 and 120 monomers, the data differentiate at the end and do not exactly follow a master curve anymore. The 120 monomer chains deviate earlier at 6000 time units compared to 7000 units of the 100's. It is also observed that low index Rouse modes start to leave the master curve earlier and deviate further at lower values. All

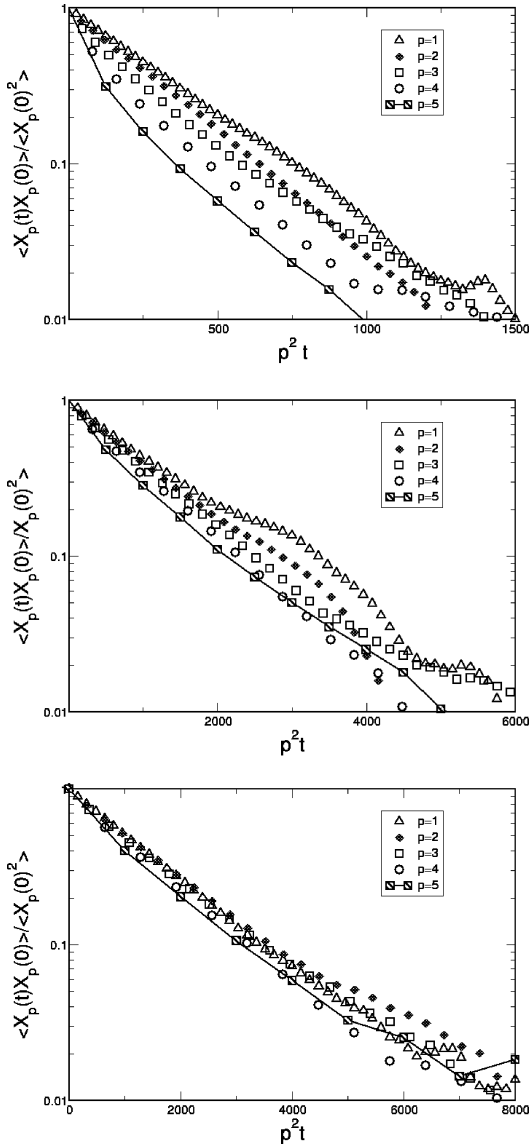

Figure 12. Time-dependent Rouse modes in Rouse scaling at chain length of 40, 70, and 80 from top.

the data suggest that for chain lengths lower than entanglement length, the systems follow the Rouse behavior if a minimum chain length is reached. The first Rouse modes of the same system are plotted in Figure 14a to understand the relaxation of the large scale vectors. It is clear that the decay of longer chains is much slower than the shorter chains. The Rouse model proposes that the Rouse time, the decay time of the first mode, of entire chains in a melt is proportional to the square of the degree of polymerization N.[33] Scaling time by chain length, the initial decays almost coincide. As the relaxation time is normalized by N^2, the first modes of 70, 80, 100, and 120 monomers chains collapse into a single curve as shown in Figure 14b. The curve for 40 monomers deviates strongly from the rest. So the chains of length 40 are not polymers in their true sense yet. As the 240 monomers are far above the entanglement length, so the Rouse model does not qualify to describe their dynamic behavior on large scales any more.

The Rouse times calculated from the $p = 1$ vector in the Rouse mode analysis are consistent with the earlier estimates from the crossover times in the mean-square displacement, e.g., at 40 monomers we find by Rouse mode analysis a time of $\tau_R = 380$. For other chain length the differences are typically 25%.

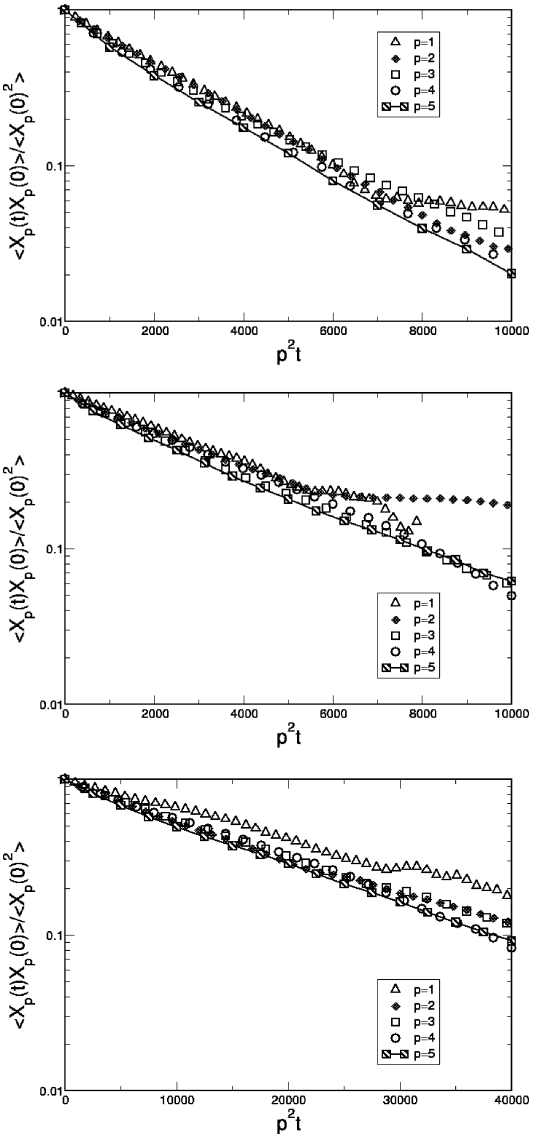

Figure 13. Time-dependent Rouse modes in Rouse scaling at chain length of 100, 120, and 240 from top.

To validate the dynamics of the mesoscale model, the Rouse modes of the 15 monomers from mesoscale model are analyzed and compared with those of the atomistic model. Figure 15 shows that there are clear deviations from Rouse behavior in both cases. To estimate the magnitude of the unit time of the mesoscale model, we calculate the reorientation times of the end-to-end vector ($p = 1$) from both models. Simulation results show that the unit time is about 150−200 ps. Mapping makes it possible to investigate the dynamics of longer chains as the atomistic simulation cannot fully relax even after 20 ns. Additionally, our mesoscale model is superior to simple bead−spring model in that it keeps the identity of PS which is achieved by employment of an extensive numerical potential.

4. Conclusion

We successfully obtained a mesoscale model of polystyrene by collecting the bond, angle, and nonbonded interaction parameters from atomistic simulations. The nonbonded numerical potential with IBI is iterated until the newly generated RDF from the mesoscale model well consistent with the atomistic one within tolerance.

Simulation results show that $\langle R_g^2 \rangle$ is proportional to N while $\tilde{l}$ and R_k are constant as well as τ_{end} and τ_{local} increase with the chain length. Investigations of mean-squared displacement, diffusion constant, and Rouse mode analysis provide an

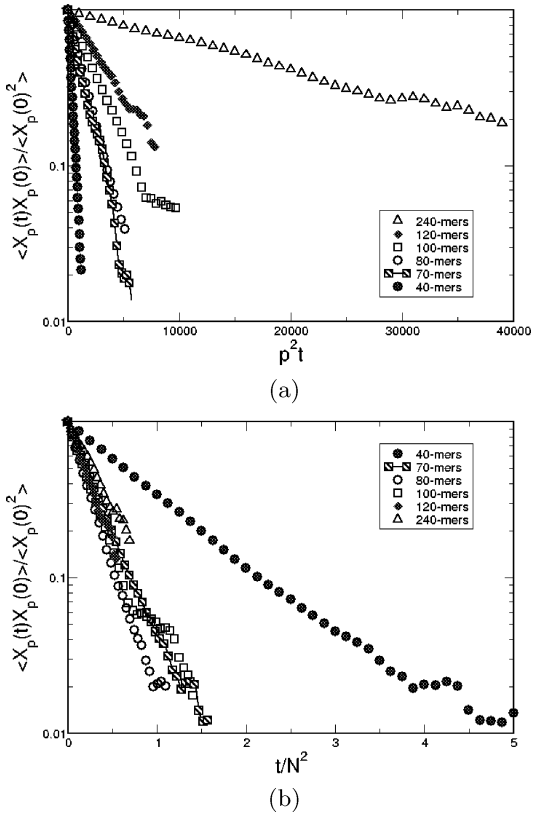

Figure 14. (a) Time-dependent first Rouse mode analysis at various chain length. (b) Time-dependent first Rouse mode scaled by the square of the degree of polymerization N^2 at various chain lengths.

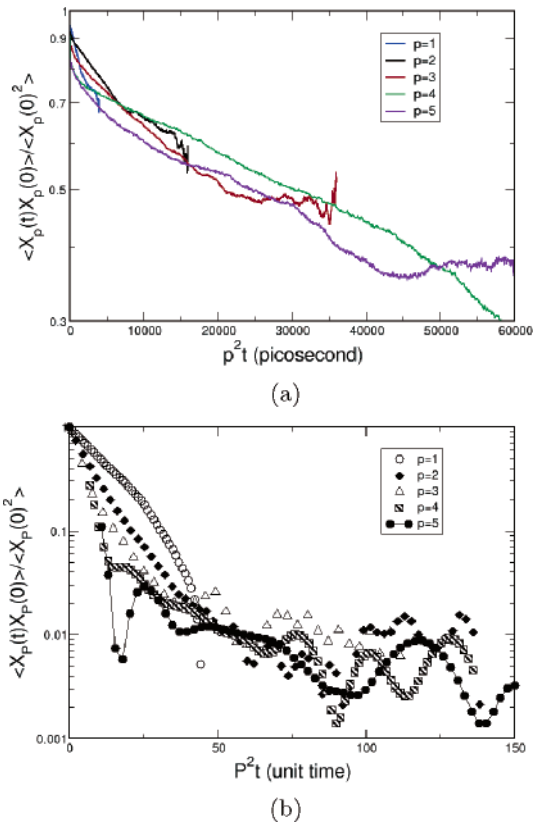

Figure 15. Rouse mode analysis at chain length of 15: (a) from atomistic scale; (b) from mesoscale.

extensive description of the transition from unentangled to entangled motion. A Rouse dynamics is observed from 50 to 80 monomers. We cannot observe the Rouse behaviors in the case of shorter chains since they are only oligomers. The dynamics of chain length 90, 100, 120, 160, and 240 show increasingly trends toward reptation. The relaxation times increase dramatically with the chain length, and the local end vectors decay faster than the middle ones.

It is the first time to calculate an entanglement length directly for a systematically coarse-grained melt. Our analysis provides persistent evidence for the conclusion that the entanglement length of this coarse-grained PS model is about 85 monomers, which is not too far below the experimental value of about $N_e \sim 130$. This coarse-grained model enables us to determine the dynamic behaviors of polymers of chain length which are not reachable in atomistic simulations.

Acknowledgment. Financial support from the U.S. Department of Energy, Office of Advanced Scientific Computing, under Grant DE-FG02-03ER25568 is gratefully acknowledged.

References and Notes

(1) Binder, K.; Cicotti, G. *Monte Carlo and Molecular Dynamics of Condensed Matter System; Como Conference Proceedings*; Oxford University Press: Bologna, 1996.
(2) Schmidt-Rohr, K.; Spiess, H. W. *Multidimensional Solid-State NMR and Polymers*; Academic Press: New York, 1994.
(3) Callaghan, P. T.; Samulski, E. T. *Macromolecules* **1998**, *31*, 3693−3705.
(4) Adams, C. H.; Brereton, M. G.; Ries, M. E.; Nicholson, T. M.; Hutchings, L. R.; Richards, R. W. *Macromolecules* **1998**, *31*, 8871−8877.
(5) Parrat, D.; Sommer, F.; Solleti, J. M.; Due, T. M. *J. Trace Microprobe Tech.* **1995**, *13*, 343−352.
(6) Dlubek, G.; Fretwell, H. M.; Alam, A. *Phys. Status Solidi A* **1998**, *167*, R13−R14.
(7) Nicolai, T.; Prochazka, F.; Durand, D. *Phys. Rev. Lett.* **1999**, *82*, 863−866.
(8) Pütz, M.; Kremer, K.; Grest, G. S. *Europhys. Lett.* **2000**, *49*, 735−741.
(9) Kremer, K.; Grest, G. S. *J. Chem. Phys.* **1990**, *92*, 5057−5086.
(10) Faller, R.; Müller-Plathe, F. *ChemPhysChem* **2001**, *2*, 180−184.
(11) Faller, R.; Müller-Plathe, F.; Heuer, A. *Macromolecules* **2000**, *33*, 6602−6610.
(12) Barsky, S.; Slater, G. W. *Macromolecules* **1999**, *32*, 6348−6358.
(13) Faller, R.; Reith, D. *Macromolecules* **2003**, *36*, 5406−5414.
(14) McCoy, J. D.; Curro, J. G. *Macromolecules* **1998**, *31*, 9362−9368.
(15) Tschöp, W.; Kremer, K.; Batoulis, J.; Brger, T.; Hahn, O. *Acta Polym.* **1998**, *49*, 61−74.
(16) Eilhard, J.; Zirkel, A.; Tschöp, W.; Hahn, O.; Kremer, K.; Schrpf, O.; Richter, D.; Buchenau, U. *J. Chem. Phys.* **1999**, *110*, 1819−1830.
(17) Baschnagel, J.; Binder, K.; Doruker, P.; Gusev, A. A.; Hahn, O.; Kremer, K.; Mattice, W. L.; Müller-Plathe, F.; Murat, M.; Paul, W.; Santos, S.; Suter, U. W.; Tries, V. *Adv. Polym. Sci.* **2000**, *152*, 141−156.
(18) Meyer, H.; Biermann, O.; Faller, R.; Reith, D.; Müller-Plathe, F. *J. Chem. Phys.* **2000**; *113*, 6264−6275.
(19) Haire, K. R.; Carver, T. J.; Windle, A. H. *Comput. Theor. Polym. Sci.* **2001**, *11*, 17−28.
(20) Abrams, C. F.; Kremer, K. *J. Chem. Phys.* **2002**, *116*, 3162−3165.
(21) Faller, R.; Müller-Plathe, F. *Polymer* **2002**, *43*, 621−628.
(22) Akkermans, R. L. C.; Briels, W. J. *J. Chem. Phys.* **2001**, *114*, 1020−1031.
(23) Reith, D.; Pütz, M.; Müller-Plathe, F. *J. Comput. Chem.* **2003**, *24*, 1624−1636.
(24) Colhoun, F. L.; Armstrong, R. C.; Rutledge, G. C. *Macromolecules* **2002**, *35*, 6032−6042.
(25) Robyr, P.; Tomaselli, M.; Grob-Pisano, C.; Meier, B. H.; Ernst, R. R.; Suter, U. W. *Macromolecules* **1995**, *28*, 5320−5324.
(26) He, Y.; Lutz, T. R.; Ediger, M. D.; Ayyagari, C.; Bedrov, D.; Smith, G. D. *Macromolecules* **2004**, *37*, 5032−5039.
(27) Lyulin, A. V.; Balabaev, N. K.; Michels, M. A. J. *Macromolecules* **2002**, *35*, 9595−9604.
(28) Müller-Plathe, F. *Chem. Phys. Lett.* **1996**, *252*, 419−424.
(29) Ayyagari, C.; Bedrov, D.; Smith, G. D. *Macromolecules* **2000**, *33*, 6194−6199.
(30) Harmandaris, V. A.; Mavrantzas, V. G.; Theodorou, D. N.; Kröger, M.; Ramirez, J.; Öttinger, H. C.; Vlassopoulos, D. *Macromolecules* **2003**, *36*, 1376−1387.
(31) León, S.; van der Vegt, N.; Site, L. D.; Kremer, K. *Macromolecules* **2005**, *38*, 8078−8092.
(32) Rouse, P. E. *J. Chem. Phys.* **1953**, *21*, 1272−1280.
(33) Strobl, G. R. *The Physics of Polymers: Concepts for Understanding Their Structures and Behavior*, 2nd ed.; Springer: Berlin, 1997.
(34) Doi, M.; Edwards, S. F. *The Theory of Polymer Dynamics*; *International Series of Monographs on Physics Vol. 73*; Clarendon Press: Oxford, 1986.
(35) Jorgensen, W. L.; Severance, D. L. *J. Am. Chem. Soc.* **1990**, *112*, 4768.
(36) Müller-Plathe, F. *Macromolecules* **1996**, *29*, 4782−4791.
(37) Sun, Q.; Faller, R. *J. Phys. Chem. B* **2005**, *109*, 15714−15723.
(38) Berendsen, H. J. C.; Postma, J. P. M.; van Gunsteren, W. F.; DiNola, A.; Haak, J. R. *J. Chem. Phys.* **1984**, *81*, 3684.
(39) Lindahl, E.; Hess, B.; van der Spoel, D. *J. Mol. Mod.* **2001**, *7*, 306−317.
(40) Faller, R. *Polymer* **2004**, *45*, 3869−3876.
(41) Sun, Q.; Faller, R. *Comput. Chem. Eng.* **2005**, *29*, 2380−2385.
(42) Tschöp, W.; Kremer, K.; Batoulis, J.; Bürger, T.; Hahn, O. *Acta Polym.* **1998**, *49*, 61−74.
(43) Allen, M. P.; Tildesley, D. J. *Computer Simulation of Liquids*; Oxford University Press: New York, 1987.
(44) Sayle, R. A.; Milnerwhite, E. J. *Comput. Corner* **1995**, *20*, 374−376.
(45) Kratky, O.; Porod, G. *Recl. Trav. Chim. Pays-Bas* **1949**, *68*, 1106−1122.
(46) Fetters, L. J.; Lohse, D. J.; Richter, D.; Witten, T. A.; Zirkel, A. *Macromolecules* **1994**, *27*, 4639−4647.
(47) Faller, R. *Macromolecules* **2004**, *37*, 1095−1101.

MA0514774